FINITE DIFFERENCE METHOD FOR STOKES EQUATIONS: MAC SCHEME

LONG CHEN

In this notes, we present the most popular finite difference method, MAC [4], for the Stokes equations and analyze the MAC scheme from different prospects. We shall consider the steady-state Stokes equations

$$\begin{cases} -\Delta \boldsymbol{u} + \nabla p = \boldsymbol{f} & \text{in } \Omega, \\ -\nabla \cdot \boldsymbol{u} = g & \text{in } \Omega. \end{cases} \tag{1}$$

Here for the sake of simplicity, we fix the viscosity constant $\mu = 1$. Various boundary conditions will be provided during the discussion.

1. MAC DISCRETIZATION

Let $\boldsymbol{u} = (u, v)$ and $\boldsymbol{f} = (f_1, f_2)$. We rewrite the Stokes equations into coordinate-wise

$$-\Delta u + \partial_x p = f_1, \tag{2}$$

$$-\Delta v + \partial_y p = f_2, \tag{3}$$

$$-\partial_x u - \partial_y v = g. \tag{4}$$

The domain $\Omega = (0,1)^2$ is decomposed into small squares with size h. We use two dimensional uniform grids for $\Omega = (0,1)^2$ as a typical setting. Generalization to domains composed by rectangles and to three dimensional domains composed by cubes is straightforward but with extra notation.

Standard central difference discretization of Δ and ∂_x, ∂_y at vertices of the uniform grid will not give a stable discretization of Stokes equations due to the failure of the discrete inf-sup condition. To see this, one can view the 5-point stencil as using P_1 element for Laplacian operator and thus discretization at grid points is equivalent to use $P_1 - P_1$ unstable pair. Similarly changing pressure discretization to centers of cells corresponds to $P_1 - P_0$ which is not stable neither.

The idea of MAC, Marker and Cell, is to place the unknown of (u, v, p) in different locations. Specifically the pressure p is located in the center of each cell and the x-component velocity u on the middle points of vertical edges (red dots) and the y-component velocity v on middle points of horizontal edges; see Figure 1.

The MAC scheme is to discretize the x-coordinate momentum equation (2) at vertical edges, the y-coordinate momentum equation (3) at horizontal edges, and the continuity equation (4) at cell centers using central difference schemes.

Let us introduce the indices system consistent to the matrix, which is easier for the programming: i is the row index and j is the column index, running from $1:n$ or $1:n+1$, where n the number of cells in one direction. The pressure is then discretized to a matrix `p(1:n,1:n)`, and the velocity is `u(1:n,1:n+1)`, and `v(1:n+1,1:n)`. One can easily write out the mapping from the index (i, j) to the coordinate (x_j, y_i) for different variables. Note that it is not consistent with the traditional indices system where i for x_i and j for

Date: Create: Winter 2012. Last update: March 23, 2022.

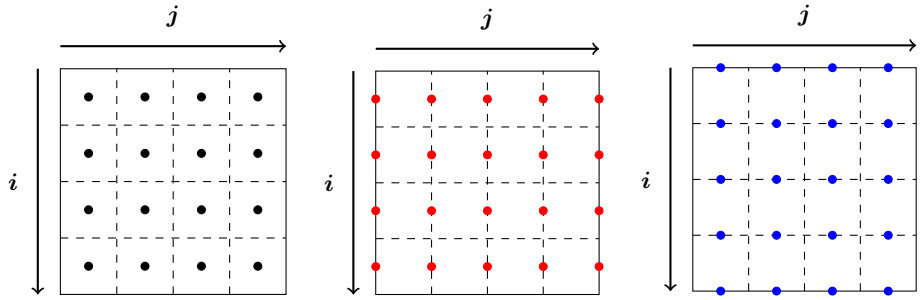

(a) p (b) u (c) v

FIGURE 1. Location and indices of (u, v, p) variables.

y_j. The advtange to use the proposed index system is that once the mapping (algebraic to geometry mapping) is fixed, in almost all places of coding, we operate on the matrix and such index system is more intuitive to traverse in the matrix. See Programming of Finite Difference Methods for detailed discussion.

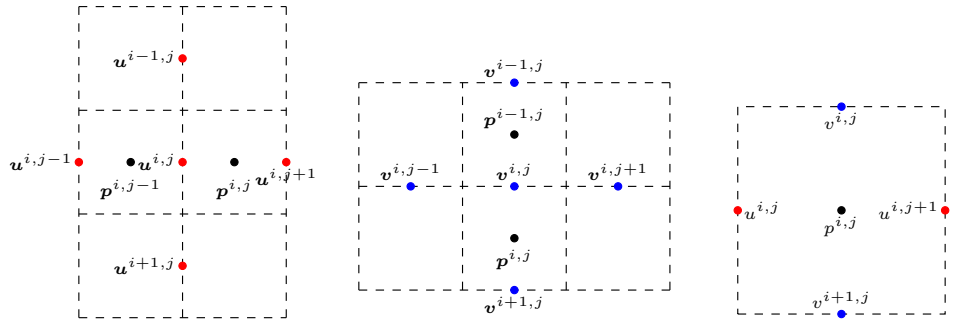

(A) equation for u **(B)** equation for v **(C)** equation for p

FIGURE 2. Indices of local stencils of MAC equations

Using this index system, the MAC scheme can be written as

$$\frac{4u^{i,j} - u^{i-1,j} - u^{i+1,j} - u^{i,j-1} - u^{i,j+1}}{h^2} + \frac{p^{i,j} - p^{i,j-1}}{h} = f_1^{i,j} \tag{5}$$

$$\frac{4v^{i,j} - v^{i-1,j} - v^{i+1,j} - v^{i,j-1} - v^{i,j+1}}{h^2} + \frac{p^{i-1,j} - p^{i,j}}{h} = f_2^{i,j} \tag{6}$$

$$-\frac{u^{i,j+1} - u^{i,j}}{h} - \frac{v^{i,j} - v^{i+1,j}}{h} = g^{i,j} \tag{7}$$

Since central difference schemes are used, it is easy to see that the above scheme has second order truncation error at interior nodes.

We then discuss discretization of boundary conditions. For Dirichlet boundary condition, one can impose it in one direction by fixing the value laying on the boundary and by extrapolation on the other direction. Let us take x-coordinate component velocity u as an example. On edges $x = 0$ and $x = 1$, the value is given by the boundary condition and no

equation is discretized on these points. On edges $y = 0$ and $y = 1$, however, there is no unknowns of u on that edge and we need to modify the stencil at $y = h/2, 1 - h/2$. As an example, consider the discretization at the index $(1, j)$. We introduce the ghost value at $y = 1 + h/2$, i.e. $u(0, j)$. Then we can discretize the momentum equation at $(1, j)$ using (5). The ghost value can be eliminated by the linear extrapolation, i.e, requiring $(u^{0,j} + u^{1,j})/2 = u_D(x_j, 1)$. Therefore the modified discretization (5) is

$$\frac{5u^{1,j} - u^{2,j} - u^{1,j-1} - u^{1,j+1}}{h^2} + \frac{p^{1,j} - p^{1,j-1}}{h} = f_1^{1,j} + \frac{2u_D(x_j, 1)}{h^2}.$$

In short

$$(5, -1, -1, -1, -2) \tag{8}$$

is the stencil for u-unknowns near the horizontal boundaries.

We can also use the quadratic extrapolation, i.e., use $u^{1/2,j}, u^{1,j}, u^{2,j}$ to fit a quadratic function and evaluate at $u^{0,j}$ to get $u^{0,j} = -2u^{1,j} + \frac{1}{3}u^{2,j} + \frac{8}{3}u^{1/2,j}$. The modified boundary scheme is:

$$\frac{6u^{1,j} - \frac{4}{3}u^{2,j} - u^{1,j-1} - u^{1,j+1}}{h^2} + \frac{p^{1,j} - p^{1,j-1}}{h} = f_1^{1,j} + \frac{\frac{8}{3}u_D(x_j, 1)}{h^2}.$$

and this near boundary stencil is denoted by

$$(6, -\frac{4}{3}, -1, -1, -\frac{8}{3}). \tag{9}$$

The quadratic extrapolation will lead to a better accuracy and the detailed error analysis can be found in Section 3. It will, however, destroy the symmetry of the matrix since the coefficient connecting $u^{1,j}$ to $u^{2,j}$ is $-4/3$ not -1.

For Neumann boundary condition $\partial u/\partial n|_{\partial\Omega} = g_N$, the ghost value will be eliminated by the central difference discretization $(u^{0,j} - u^{1,j})/h = g_N(x_j, 1)$ and the modified stencil is

$$\frac{3u^{1,j} - u^{1,j-1} - u^{1,j+1} - u^{2,j}}{h^2} + \frac{p^{1,j} - p^{1,j-1}}{h} = f_1^{1,j} + \frac{g_N(x_j, 1)}{h}.$$

Unlike the Dirichlet boundary condition, similar modification is needed for all grids points on or near the boundary edges and for points near corners two ghost degree of freedom (dof) should be introduced; see Finite Difference Methods.

We can write the discrete problem in the matrix form with familiar notation:

$$\begin{pmatrix} A & B^\intercal \\ B & 0 \end{pmatrix} \begin{pmatrix} \boldsymbol{u}_h \\ p_h \end{pmatrix} = \begin{pmatrix} \boldsymbol{f}_h \\ g_h \end{pmatrix}, \tag{10}$$

where $A = -\Delta$ and $B = -\operatorname{div}$. There is no need to form these matrices when implement the MAC scheme. See the matrix-free implementation in Programming of MAC Scheme for Stokes Equations.

Exercise 1.1. Verify the matrix $BB^\intercal$ is the standard 5-point stencil of Laplacian operator discretized at cell centers and with Neumann boundary conditions. Therefore the pressure is unique up to a constant.

2. Covolume Formulation

We shall interpret MAC from covolume formulation.

2.1. **Concepts from algebraic topology.** An n-dimensional closed cell is a domain that is homeomorphic to an n-dimensional closed ball. Examples of cells includes simplex, cubes, rectangles, and all polyhedra. In algebraic topology, prefix is added to distinguish cells in different dimensions. We shall use conventional names when possible. Namely vertices or nodes for 0-cell, edge for 1-cell, face for 2-cell, and volume for 3-cell. With a slight abuse of notation, we still use "cell" for the cell with the highest dimension in the grid.

Cell complex $\mathcal{K}$ is a collection of cells satisfying conforming property: 1. any face of a cell in $\mathcal{K}$ is also in $\mathcal{K}$; 2. the intersection of any two cells is a common face of these two cells. A simplicial complex is a cell complex whose cells are all simplices. For a grid to be a cell complex, it should be a conforming grid (without overlapping or hanging nodes) and in the cell complex of this grid, all lower dimensional cells are included. The body $|\mathcal{K}|$ of a complex $\mathcal{K}$ is the union of all cells. When a subset Ω of $\mathbb{R}^n$ is the body of a cell complex $\mathcal{K}$, then $\mathcal{K}$ is said to be a mesh (or grid) of Ω. In the rest, we shall mainly work on 2-dimensional grids and its corresponding cell complex.

In a 2-D cell complex, each cell will be oriented counterclockwise. For an oriented cell T, its boundary will inherit a induced orientation. Each edge will assign a direction as its orientation. Note that for two counterclockwise oriented cells T_1, T_2 sharing one edge e, if the direction of e is consistent with the induced orientation from T_1, then it is opposite to that induced from T_2. The orientation of a node is defined as positive if a vector point to this node and negative if a vector leaving this node. A good example is the notation when evaluating an integral $u|_0^1 = u|_{\partial(0,1)}$.

For a d-cell T, ∂T consists of $d-1$-cells on the boundary of T. Taking the orientation into consideration, we write 1 if the orientation is consistent and -1 if not. Therefore we can write a formal linear combination

$$\partial T = e_1 + e_2 - e_3.$$

More generally, let us label each oriented d-cell with a superscript univocally identifying it. We define a chain (with integer coefficients) as a formal addition of cells c_i with integer coefficients n_i

$$C = \sum_i n_i c^i.$$

The boundary operator ∂ can be linearly extended to a chain, i.e., $\partial C = \sum_i n_i \partial c^i$.

All d-dimensional chains forms an abelian group (or a module) $\mathcal{C}_d$ with generators $\{c^i\}$. Relative to these generators, a chain can be identified as a vector. The boundary operator will then have a matrix representation which is the transpose of the incidence matrix introduced below. In abstract definition, an incidence matrix is a matrix that shows the relationship between two classes of sets: X and Y. The matrix $R_{XY} = (r_{xy})$ is of size $N_X \times N_Y$ and $r_{xy} = 1$ if x and y are related (called incident in this context) and 0 if they are not. For $X = \{c_d^i\}$ and $Y = \{c_{d-1}^i\}$ consisting of orientated cells, when y is a face of x, we refine the definition to $r_{xy} = 1$ with the consistent orientation and $r_{xy} = -1$ if the orientation is inconsistent. Now it is straightforward to verify that $\partial_d = R_{XY}^{\intercal} = R_{YX}$.

All chains groups and boundary operators forms a chain complex

$$\mathcal{C}_n \xrightarrow{\partial_n} \mathcal{C}_{n-1} \cdots \mathcal{C}_1 \xrightarrow{\partial_1} \mathcal{C}_0 \longrightarrow 0.$$

The last 0 represents the trivial group. Note that $\partial_d \circ \partial_{d+1} = 0$ which implies $\mathrm{img}(\partial_{d+1}) \subseteq \ker(\partial_d)$ and the factor group

$$H_d(\Omega) = \ker(\partial_d)/\mathrm{img}(\partial_{d+1})$$

is called the d-th homology group of Ω, the body of the cell complex. The rank of H_d is called the d-th Betti number of Ω. The first few Betti numbers have the following intuitive definitions:

- b_0 is the number of connected components;
- b_1 is the number of two-dimensional or "circular" holes;
- b_2 is the number of three-dimensional holes or "voids".

A domain is simply connected if $b_1 = 0$. For 2-D domains, it is equivalent to no holes. But a 3-D domain with a three-dimensional holes could be still simply connected.

2.2. **Cell complex of primary and dual grids.** The unit square is decomposed into $N = n^2$ small squares with size h. This grid is called the primary grid and denoted by $\mathcal{T}_h$. The subscript h is used to record the mesh size. We will omit the subscript when necessary. The center of the boundary cells are reflected (relative to nearby boundary edge and corners). The centers of all cells including these reflected form another grid consisting of squares with size h which will be called the dual grid and denoted by $\bar{\mathcal{T}}_*$. Due to the reflected centers, the dual grid will cover the primary grid. •1 Cells in $\bar{\mathcal{T}}_*$ with non-empty intersection with the boundary of the domain will be called (dual) boundary cells and other cells will be called interior cells and denoted by $\mathcal{T}_*$.

•1 *figure here*

Each cell in the dual grid forms a covolume of the vertices in the primary grid. More generally, cells in $\mathcal{T}_*$ is isomorphism to $\mathcal{T}$ by a one-to-one mapping between a k-cell in $\mathcal{T}_*$ and a $(d-k)$-cell in $\mathcal{T}$ (will be referred as dual cells). For rectangular grids, the dual cells are orthogonal and intersect at barycenters. This orthogonality and symmetry leads to special duality for the discretization of differential operators on rectangular grids. For triangular grids, the orthogonality and part of the symmetry can be preserved using Delaunay-Voronoi dual grids which imposes certain geometric restriction on grids. For general triangular grids and its dual grids formed by barycenters, the orthogonality is lost. Consequently discretization on unstructured grids is harder than rectangular grids.

All cells will be oriented counterclockwise. For a 2-D cell complex, we should be careful on the orientation of edges. First treat as the boundary face of 2-cells, its orientation is given by the normal vector; see the figure below. On the other hand, as a 1-cell, the orientation could be given by the tangential vector. In 3-D, such distinguish will be more clear since the first one is the normal direction of faces but in 2-D both normal and tangential direction are associated to edges. One can always rotate the normal direction 90° to get a tangential direction.

For the primary grid, the edge will be assign a normal orientation and on the dual grid the tangential orientation. Thus on the primary cell, an edge is consistent with the cell if its normal orientation is the outwards normal direction of the cell.

2.3. **Differential operators in two dimensions.** Besides the gradient and divergence operator, we will use two more differential operators curl and rot in $\mathbb{R}^2$. The curl operator is unambiguously defined for a 3-D vector fields $\boldsymbol{v}$ and the result $\operatorname{curl} \boldsymbol{v}$ is still a 3-D vector field. When restricted to 2-D, we have two variants. For a scalar function ϕ, treating it as $(0, 0, \phi)$ and taking curl, we get a 3-D vector field which can be identified as a 2-D vector field since the third component is always zero

$$\operatorname{curl} \phi = (\partial_y \phi, -\partial_x \phi).$$

For a 2-D vector field $\boldsymbol{u} = (u(x, y), v(x, y))$, treating as $(u, v, 0)$ and taking curl, we get a 3-D vector with only nonzero component in the third coordinate and thus can be identified

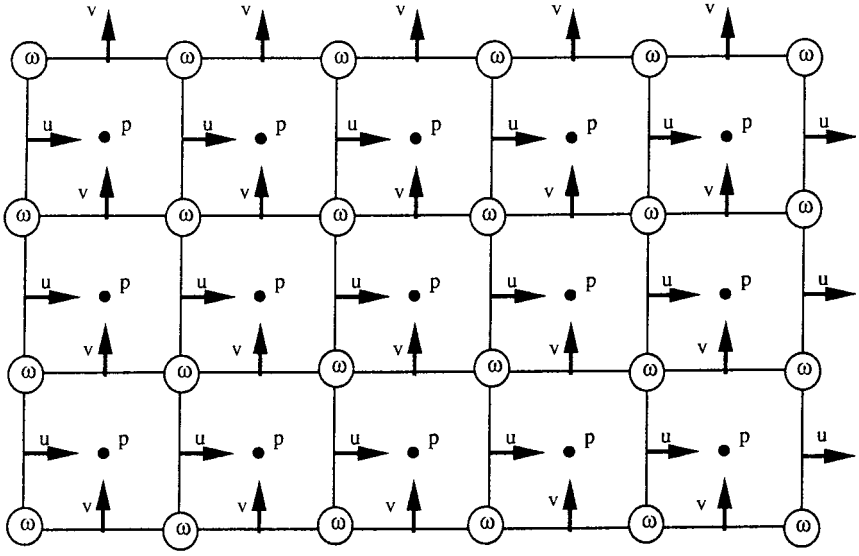

Figure 1. Marker and cell discretization on a Cartesian mesh.

FIGURE 3. Figures extracted from Dubois. Vorticity–velocity–pressure formulation for the Stokes problem. Mathematical methods in the applied sciences. 25(13):1091–1119, 2002.

as a scalar

$$\operatorname{rot} \boldsymbol{u} = \partial_x v - \partial_y u.$$

In 2-D, if we introduce the clockwise 90° rotation and use $\perp$ in the superscript to denote this rotation, then

$$\operatorname{curl} f = (\operatorname{grad} f)^\perp, \ \operatorname{rot} \boldsymbol{u} = \operatorname{div} \boldsymbol{u}^\perp.$$

We summarize these differential operators in the following exact sequence

$$\mathcal{C}^1(\Omega) \underset{\text{rot}}{\overset{\text{curl}}{\rightleftharpoons}} \mathcal{C}^1(\Omega) \underset{\text{grad}}{\overset{\text{div}}{\rightleftharpoons}} \mathcal{C}^1(\Omega). \tag{11}$$

The above sequence is exact since the composition of consecutive operators vanishes.

2.4. **Discrete vector fields and differential operators.** The pressure can be treat as a function on 2-chain $\mathcal{C}_2(\mathcal{T})$ (or in general n-chain $\mathcal{C}_n$ in $\mathbb{R}^n$) and the velocity $\boldsymbol{u}$ is a function on 1-chain $\mathcal{C}_1(\mathcal{T})$ (in general $n-1$-chain $\mathcal{C}_{n-1}$ in $\mathbb{R}^n$). To respect the convention of finite difference methods, we treat the discrete fields as point-wise evaluation at barycenters of cells (center of 2-cells or middle points of edges). A more rigorous one is to use the terminology differential form, which is an appropriate line or surface integral, in the algebraic topology and will be discussed later.

The velocity $\boldsymbol{u} = (u, v)$ can be understood as the boundary normal flux $\boldsymbol{u} \cdot \boldsymbol{n}$ of the primary cell and the tangential velocity $\boldsymbol{u} \cdot \boldsymbol{t}$ on the dual cell evaluated at the middle points of edges. Therefore we can discretize $\operatorname{div} \boldsymbol{u}$ at the cell centers of the primary grid and $\operatorname{rot} \boldsymbol{u}$, which is known as vorticity ω, on the dual grid.

We use notation $\mathcal{D}$ for div and $\mathcal{C}_*$ for curl on the dual grid. The discrete gradient of press p is the forward finite difference on the dual grid and denoted by $\mathcal{G}_*$. The cell on the primary and dual grid will be denoted by T and T_*. In the finite difference setting, the first order differential matrix is of the scaling $1/h$ and the second one Δ is $1/h^2$.

The discrete vector fields can be identified as a vector formed by the function value at centers. Therefore the differential operator will have a corresponding matrix representation and will be denoted by the same notation. For one cell, the div matrix is $(1, 1, -1, -1)/h$. It is not difficult to see the differential operator is closely related to the boundary operator and in turn the incidence matrix R_{XY}.

$$\begin{aligned}\mathcal{D} &= \partial_2^\intercal/h = R_{2,1}/h,\\ \mathcal{C} &= \partial_1^\intercal/h = R_{1,0}/h,\\ \mathcal{R}_* &= \partial_{2*}^\intercal/h = R_{2,1}^*/h\\ \mathcal{G}_* &= \partial_{1*}^\intercal/h = R_{1,0}^*/h.\end{aligned}$$

Here $R_{1,0}^*$ means the incidence matrix of the 1-cell and 0-cell on the dual grid and by the definition $R_{1,2}$ as a k-cell in the primary is dual to a $(n-k)$-cell in the dual grid. Based on that, it is easy to verify the duality of differential operators by the relation to the incidence matrix that

$$\mathcal{D} = -\mathcal{G}_*^\intercal,\ \mathcal{C} = \mathcal{R}_*^\intercal.$$

The identity in the continuous level

$$-\boldsymbol{\Delta} = -\mathrm{grad}\ \mathrm{div} + \mathrm{curl}\ \mathrm{rot}$$

is discretized as

$$-\boldsymbol{\Delta}_h = -\mathcal{D}^\intercal\mathcal{D} + \mathcal{R}_*^\intercal\mathcal{R}_* = -\mathcal{G}_*\mathcal{D} + \mathcal{C}\mathcal{R}_*. \tag{12}$$

Namely the five-point stencil can be derived from (12). See Figure 4 for such a verification for u-component. Note that this identity only holds for interior edges.

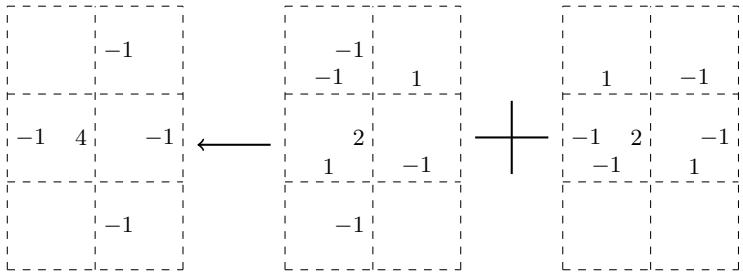

(A) $\mathcal{A}$ (B) $\mathcal{C}\mathcal{C}^t$ (C) $\mathcal{D}^t\mathcal{D}$

FIGURE 4. The five point stencil is the combination of $\mathcal{C}\mathcal{C}^\intercal + \mathcal{D}^\intercal\mathcal{D}$.

The exactness $\mathrm{div}\,\mathrm{curl} = 0, \mathrm{rot}\,\mathrm{grad} = 0$ is faithfully preserved in the discretation

$$\mathcal{D}\mathcal{C} = 0, \quad \mathcal{R}_*\mathcal{G}_* = 0, \tag{13}$$

which is just the fact $\partial_d \circ \partial_{d+1} = 0$ of chain complex in primary and dual grids.

The impose of boundary conditions will introduce complication. For Dirichlet boundary condition, part of the velocity is on the boundary.

The matrix equation of MAC can be written as

$$\begin{pmatrix} \mathcal{D}^\intercal\mathcal{D} + \mathcal{R}_*^\intercal\mathcal{R}_* & \mathcal{G}_* \\ -\mathcal{D} & 0 \end{pmatrix} \begin{pmatrix} \boldsymbol{u} \\ p \end{pmatrix} = \begin{pmatrix} \boldsymbol{f} \\ 0 \end{pmatrix}.$$

The above equations are posed on interior nodes only. To impose the boundary condition $\boldsymbol{u} = g_D$ on $\partial\Omega$, the stencil near boundary should be changed.

Use these discrete differential operator, we can easily verify

$$BB^\intercal = -\mathcal{D}\mathcal{G}_* \approx -\operatorname{div}\operatorname{grad}$$

is the standard 5 point stencil of $-\Delta$ operator for 2-cells on the primary grid with Neumann boundary condition.

We can also verify the commutator:

$$\Delta_u \operatorname{grad}_p = \operatorname{grad}_p \Delta_p. \tag{14}$$

using these notation

$$-\Delta\mathcal{G}_* = (-\mathcal{D}^\intercal\mathcal{D} + \mathcal{R}_*^\intercal\mathcal{R}_*)\mathcal{G}_* = -\mathcal{G}_*\mathcal{D}\mathcal{G}_* = -\mathcal{G}_*\Delta_p.$$

For Laplace operator with boundary condition, as the boundary stencil is changed, the commutator is non-zero for the cells near the boundary.

3. Convergence Analysis

In this section we provide convergence analysis for MAC schemes. We first present a finite element interpretation developed by Han and Wu in [3] for which the discrete inf-sup condition is easy to verify. Then we show the relation to MAC schemes and thus obtain the stability of MAC schemes. With the standard truncation error analysis, we then obtain the rate of convergence which depends on the way of imposing boundary condition. For the quadratic extrapolation, a second order convergence in H^1 norm of velocity and L^2 norm of pressure can be obtained, while for the linear extrapolation, only first order result can be proved.

Note that Han and Wu obtained only a first order convergence result for finite element formulation (20) and Nicolaides [5] proved the first order convergence for a scheme equivalent to linear extrapolation scheme (23). The second order convergence of the MAC scheme for the steady state Stokes equations seems not rigorously proved before.

Denote the number of unknowns for velocity and pressure as N_u and N_p, respectively, and the size of discrete system as $N := N_u + N_p$. The near boundary nodes for velocity is labeled from 1 to N_b and interior nodes from $N_b + 1$ to N_u.

3.1. A Finite Element Method Interpretation.

We follow the work of Han and Wu in [3] to interprete the MAC as a special finite element method. Denote $\mathbb{V} := \boldsymbol{H}_0^1(\Omega)$ as the $\boldsymbol{H}^1$ function with zero trace, and $\mathbb{Q} := L_0^2(\Omega)$ the L^2 functions with mean value zero over domain Ω. The corresponding dual spaces are $\mathbb{V}' = \boldsymbol{H}^{-1}(\Omega)$ and $\mathbb{Q}' = L_0^2(\Omega)$ respectively. The Stokes operator $\mathcal{L}$ can then be understood as $\mathcal{L} : \mathscr{X} \to \mathscr{Y}$ with $\mathscr{X} := \mathbb{V} \times \mathbb{Q}$ and $\mathscr{Y} := \mathbb{V}' \times \mathbb{Q}'$.

The variational problem for (1) reads as: find $(\boldsymbol{u}, p) \in \mathbb{V} \times \mathbb{Q}$, such that

$$\begin{cases} a(\boldsymbol{u}, \boldsymbol{v}) + b(\boldsymbol{v}, p) = (\boldsymbol{f}, \boldsymbol{v}) & \text{for all } \boldsymbol{v} \in \mathbb{V}, \\ b(\boldsymbol{u}, q) = 0 & \text{for all } q \in \mathbb{Q}, \end{cases} \tag{15}$$

where $(\cdot,\cdot)$ is the L^2-inner product and

$$a(\boldsymbol{u}, \boldsymbol{v}) = (\nabla\boldsymbol{u}, \nabla\boldsymbol{v}), \quad b(\boldsymbol{v}, q) = (-\operatorname{div}\boldsymbol{v}\, q).$$

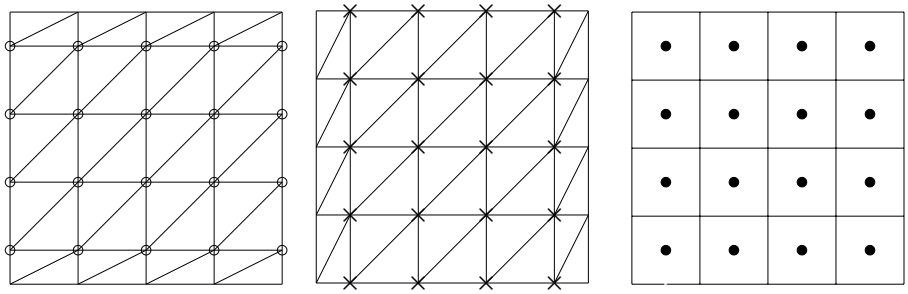

(a) Mesh $\mathcal{T}_h^1$ for u (b) Mesh $\mathcal{T}_h^2$ for v (c) Mesh $\mathcal{T}_h$ for p

FIGURE 5. The meshes for velocity and pressure

To approximate the velocity space $\mathbb{V}$ and pressure space $\mathbb{Q}$, we introduce subspaces $\mathbb{V}_h$ and $\mathbb{Q}_h$ based on three different meshes: triangulations $\mathcal{T}_h^1$, $\mathcal{T}_h^2$, and quadrangulation $\mathcal{T}_h$, as shown in Figure 5. The triangulations $\mathcal{T}_h^1$ and $\mathcal{T}_h^2$ are modified from quadrangulations in Han and Wu [3] by dividing rectangles into triangles using diagonals with positive slope.

Corresponding to the triangulations $\mathcal{T}_h^1$ and $\mathcal{T}_h^2$, we define

$$\mathbb{V}_h^1 = \{u_h \in H_0^1(\Omega) : u_h|_\tau \text{ is a linear function, for all } \tau \in \mathcal{T}_h^1\},$$
$$\mathbb{V}_h^2 = \{v_h \in H_0^1(\Omega) : v_h|_\tau \text{ is a linear function, for all } \tau \in \mathcal{T}_h^2\},$$

and denote by $\mathbb{V}_h = \mathbb{V}_h^1 \times \mathbb{V}_h^2$. Corresponding to the quadrangulation $\mathcal{T}_h$, we define

$$\mathbb{Q}_h = \{q_h \in L_0^2(\Omega) : q_h|_\tau = \text{constant, for all } \tau \in \mathcal{T}_h\}.$$

To discuss the boundary condition more conveniently, we introduce more notation. We denote the boundary of Ω as Γ. The set of nodes for the velocity is denoted by Ω_h and the boundary nodes by Γ_h. The near boundary (nb) nodes for velocity is defined as:

$$\begin{aligned}
\Gamma_{nb}^u &= \{(x,y) \text{ is a vertex of type } \circ \mid y = h/2 \text{ or } 1-h/2\},\\
\Gamma_{nb}^v &= \{(x,y) \text{ is a vertex of type } \times \mid x = h/2 \text{ or } 1-h/2\},\\
\Gamma_{nb} &= (\Gamma_{nb}^u, \Gamma_{nb}^v).
\end{aligned}$$

With a slight abuse of notation, we also use $\Gamma_{nb}^u, \Gamma_{nb}^v, \Gamma_{nb}$, Ω_h etc. to denote the indices set. The interior nodes set is defined as $\overset{\circ}{\Omega}_h = \Omega_h \backslash (\Gamma_h \cup \Gamma_{nb})$.

The discrete problem reads as: find $(\boldsymbol{u}_h, p_h) \in \mathbb{V}_h \times \mathbb{Q}_h$, such that

$$\begin{cases} a(\boldsymbol{u}_h, \boldsymbol{v}_h) + b(\boldsymbol{v}_h, p_h) = (\boldsymbol{f}, \boldsymbol{v}_h) & \text{for all } \boldsymbol{v}_h \in \mathbb{V}_h, \\ b(\boldsymbol{u}_h, q_h) = 0 & \text{for all } q_h \in \mathbb{Q}_h. \end{cases} \tag{16}$$

With appropriate numerical quadrature, we are able to get a variant of MAC scheme. It is easy to verify that the interior stencil corresponding to $a(\cdot,\cdot)$ is $(4,-1,-1,-1,-1)$. For near boundary nodes, again we take u as an example to derive the boundary stencil as shown in Figure 6.

Denote the basis at point 1 as $\boldsymbol{\phi}_1 = (\lambda_1, 0)^\intercal$, straightforward computation yields the stencil for the near boundary node 1 is

$$a(\boldsymbol{u}_h, \boldsymbol{\phi}_1) = \frac{9}{2}u_1 - u_4 - \frac{3}{4}u_2 - \frac{3}{4}u_5 - 2u_0,$$

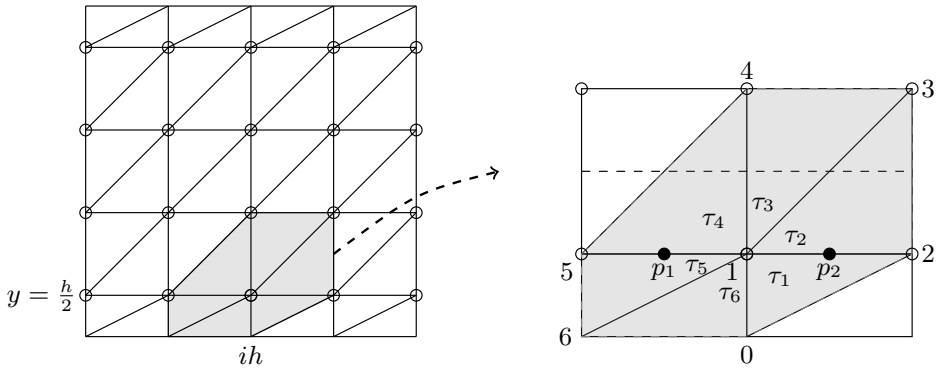

FIGURE 6. Stencil computation for the near boundary points.

and the corresponding stencil will be denoted by

$$(\frac{9}{2}, -1, -\frac{3}{4}, -\frac{3}{4}, -2). \tag{17}$$

One point quadrature at point 1 in Figure 6 is used to compute $b(\boldsymbol{\phi}_1, p_h)$:

$$b(\boldsymbol{\phi}_1, p_h) = \sum_{i=1}^{6} \int_{\tau_i} -\operatorname{div} \boldsymbol{\phi}_1 \cdot p_h \approx b_h(\boldsymbol{\phi}_1, p_h) = h(p_2 - p_1),$$

which is equivalent to use the middle point quadrature when computing $\int_e \boldsymbol{u} \cdot \boldsymbol{n} \, \mathrm{d}s$ for an edge of the cell. That is

$$b(\boldsymbol{u}_h, \chi_\tau) = -\int_\tau \operatorname{div} \boldsymbol{u}_h \, \mathrm{d}x = -\sum_{e \in \partial\tau} \int_e \boldsymbol{u}_h \cdot \boldsymbol{n} \, \mathrm{d}s \approx h(u^{i,j+1} - u^{i,j}) + h(v^{i,j} - v^{i+1,j}).$$

Define the corresponding linear operators:

$$A : \mathbb{V}_h \to \mathbb{V}_h', \text{ and } \langle A\boldsymbol{u}_h, \boldsymbol{v}_h \rangle = a(\boldsymbol{u}_h, \boldsymbol{v}_h),$$

and

$$B : \mathbb{V}_h \to \mathbb{Q}_h', B^\intercal : \mathbb{Q}_h \to \mathbb{V}_h', \text{ and } \langle B\boldsymbol{v}_h, q_h \rangle = \langle \boldsymbol{v}_h, B^\intercal q_h \rangle := b_h(\boldsymbol{v}_h, q_h).$$

And define the functional $\boldsymbol{f}_h, \boldsymbol{f}_I \in \mathbb{V}_h'$:

$$\langle \boldsymbol{f}_h, \boldsymbol{v}_h \rangle := (\boldsymbol{f}, \boldsymbol{v}_h) \text{ , for all } \boldsymbol{v}_h \in \mathbb{V}_h, \tag{18}$$

and

$$\langle \boldsymbol{f}_I, \boldsymbol{v}_h \rangle = (\boldsymbol{f}_I, \boldsymbol{v}_h)_h := \sum_{i=1}^{N_u} h^2 \boldsymbol{f}(x_i) \boldsymbol{v}(x_i) \text{ , for all } \boldsymbol{v}_h \in \mathbb{V}_h, \tag{19}$$

where x_i is the velocity nodes. The inner product $(\cdot,\cdot)_h$ is a discrete version of the L^2-inner product $(\cdot,\cdot)$ of $\mathbb{V}$. One can easily show that $(\boldsymbol{u}, \boldsymbol{u})_h \eqsim (\boldsymbol{u}, \boldsymbol{u})$ for any $\boldsymbol{u} \in \mathbb{V}$.

Using these notation, we can write the discrete problem (16) in the operator form:

$$\begin{pmatrix} A & B^\intercal \\ B & 0 \end{pmatrix} \begin{pmatrix} \boldsymbol{u}_h \\ p_h \end{pmatrix} = \begin{pmatrix} \Pi_h \boldsymbol{f} \\ 0 \end{pmatrix}. \tag{20}$$

where $(\boldsymbol{u}_h, p_h) \in \mathscr{X}_h := \mathbb{V}_h \times \mathbb{Q}_h$, $\Pi_h \boldsymbol{f} = \boldsymbol{f}_h$ or $\boldsymbol{f}_I$, and $(\Pi_h \boldsymbol{f}, 0) \in \mathscr{Y}_h := \mathbb{V}_h' \times \mathbb{Q}_h'$.

3.2. **Connection between FE and FD.** For the finite difference schemes and the finite element scheme (20), we get the same stencil for the divergence operator, and the same stencil for the interior part for the Laplacian operator. The only difference is the near boundary stencil of the Laplacian operator, which accounts for different ways of imposing the Dirichlet boundary condition. We explore their connection below.

First we define the relation between vectors and functions and that between matrices and operators. We chose the standard hat basis function for $\mathbb{V}_h$ and the characteristic functions of cells as the basis for $\mathbb{Q}_h$. Then a function can be identified as its coordinate vector and vice verse. We put an arrow to indicate this isomorphism. For example, for $\boldsymbol{u}_h \in \mathbb{V}_h$, $\vec{\boldsymbol{u}}_h \in \mathbb{R}^{N_u}$ is its coordinate vector and similarly for $p_h \in \mathbb{Q}_h, \vec{p}_h \in \mathbb{R}^{N_p}$ is its vector representation. The following identities can be used to define a matrix by a linear operator and vice verse:

$$\langle A\boldsymbol{u}_h, \boldsymbol{v}_h\rangle = \vec{\boldsymbol{v}}_h^t \vec{A}\vec{\boldsymbol{u}}_h, \tag{21}$$

$$\langle B\boldsymbol{u}_h, q_h\rangle = \vec{q}_h^t \vec{B}\vec{\boldsymbol{u}}_h. \tag{22}$$

In the rest of this notes, we will mix the usage of a matrix form or operator form which should be clear by the context.

Therefore we can rewrite the MAC schemes using operator notation

$$\begin{pmatrix} A_L & B^\intercal \\ B & 0 \end{pmatrix} \begin{pmatrix} \boldsymbol{u}_h \\ p_h \end{pmatrix} = \begin{pmatrix} \boldsymbol{f}_I \\ 0 \end{pmatrix}, \tag{23}$$

$$\begin{pmatrix} A_Q & B^\intercal \\ B & 0 \end{pmatrix} \begin{pmatrix} \boldsymbol{u}_h \\ p_h \end{pmatrix} = \begin{pmatrix} \boldsymbol{f}_I \\ 0 \end{pmatrix}. \tag{24}$$

where A_L corresponds to the stencil (8) and A_Q for (9). The corresponding Stokes operator will be denoted by $\mathcal{L}_h^l$ and $\mathcal{L}_h^q$, respectively.

We can now show the connection between finite difference methods and the finite element method using these notation. For the linear extrapolated finite difference scheme (23), we denote $A_\Gamma = A_L - A$. By direct calculation, $\vec{A}_\Gamma$ has stencil $(\frac{1}{2}, -\frac{1}{4}, -\frac{1}{4})$ on Γ_{nb} and equal to zero on all other parts.

For the quadratic extrapolated finite difference scheme (24), we denote matrix $\vec{D}$:

$$\vec{D} = \vec{I} \quad \text{in} \quad \mathring{\Omega}_h, \quad \vec{D} = \frac{4}{3}\vec{I} \quad \text{on } \Gamma_{nb}. \tag{25}$$

Then we can easily verify the relation: $\vec{A}_Q = \vec{D}\vec{A}$ by the stencil (9) and (17).

We shall prove the stability of schemes (23) and (24) by the stability results of finite element method presented in [3] using these relations.

3.3. **Stability of MAC Schemes.** Following results of Lemma 4 and Lemma 6 in [3], we have the stability of the finite element scheme as below. For completeness, we sketch a proof below.

Lemma 3.1. *There exists $\alpha, \beta > 0$ independent of h, such that*

$$\inf_{\boldsymbol{v}_h\in\mathbb{V}_h} \sup_{\boldsymbol{u}_h\in\mathbb{V}_h} \frac{\langle A\boldsymbol{u}_h, \boldsymbol{v}_h\rangle}{\|\boldsymbol{u}_h\|_A\|\boldsymbol{v}_h\|_A} = \inf_{\boldsymbol{u}_h\in\mathbb{V}_h} \sup_{\boldsymbol{v}_h\in\mathbb{V}_h} \frac{\langle A\boldsymbol{u}_h, \boldsymbol{v}_h\rangle}{\|\boldsymbol{u}_h\|_A\|\boldsymbol{v}_h\|_A} = \alpha, \tag{26}$$

$$\inf_{q_h\in\mathbb{Q}_h} \sup_{\boldsymbol{v}_h\in\mathbb{V}_h} \frac{\langle q_h, B\boldsymbol{v}_h\rangle}{\|q_h\|\|\boldsymbol{v}_h\|_A} = \beta. \tag{27}$$

Proof. The inf-sup condition for A is trivial since $\langle A\boldsymbol{u}_h, \boldsymbol{v}_h\rangle = (\nabla \boldsymbol{u}_h, \nabla \boldsymbol{v}_h)$ is an inner product on $\boldsymbol{H}_0^1$.

The inf-sup condition for B is more involved. For a given q_h, the inf-sup condition in the continuous level is applied to find $\boldsymbol{v} \in \boldsymbol{H}_0^1$ such that $\operatorname{div} \boldsymbol{v} = q_h$ and $\|\boldsymbol{v}\|_A \lesssim \|q_h\|$. Then a bounded Fortin operator $I_h : H_0^1 \to \mathbb{V}_h$ is defined such that $\operatorname{div} \boldsymbol{v} = \operatorname{div} I_h \boldsymbol{v}$, and $\|I_h \boldsymbol{v}\|_A \lesssim \|\boldsymbol{v}\|_A$. Let $\boldsymbol{v}_h = I_h \boldsymbol{v}$, then we have $\operatorname{div} \boldsymbol{v}_h = q_h$ and $\|\boldsymbol{v}_h\|_A \lesssim \|q_h\|$.

To define a Fortin operator, we first apply the integration by parts and write

$$\int_\tau \operatorname{div} \boldsymbol{u} \,\mathrm{d}x = \int_{\partial\tau} \boldsymbol{u}\cdot\boldsymbol{n} \,\mathrm{d}s.$$

On the vertical edges, we define the nodal value on $\mathcal{T}_h^1$ as the average of the integral of x-component of velocity, i.e. $u_h(x_i, y_j)h = \int_e u \,\mathrm{d}s$. Similarly we define y-component of velocity $v_h(x_i, y_j)h = \int_e v \,\mathrm{d}s$. Therefore the boundary integral are preserved and consequently

$$b_h(\boldsymbol{u}_h, \chi_\tau) = b(\boldsymbol{u}, \chi_\tau).$$

The H^1-stability of such operator can be proved similarly as that in $P_1^{\mathrm{CR}} - P_0$ pairs for Stokes equations; see *Chapter: Finite element method for Stokes equations*. □

The inf-sup condition of A_L is based on the following norm equivalence. The finite difference scheme is fitted into the finite element space, so that the trace theorem which plays an essential role in the proof can be applied.

Lemma 3.2. *The norm defined by A_L is equivalent to the norm defined by A, that is:*

$$\langle A\boldsymbol{u}_h, \boldsymbol{u}_h\rangle \leq \langle A_L\boldsymbol{u}_h, \boldsymbol{u}_h\rangle \lesssim \langle A\boldsymbol{u}_h, \boldsymbol{u}_h\rangle. \tag{28}$$

Consequently, the bilinear form $\langle A_L\boldsymbol{u}, \boldsymbol{v}\rangle$ is stable in $\|\cdot\|_A$.

Proof. Recall that $\vec{A}_L = \vec{A} + \vec{A}_\Gamma$ with $\vec{A}_\Gamma = (\frac{1}{2}, -\frac{1}{4}, -\frac{1}{4})$ on Γ_{nb}. Therefore

$$\langle A_L\boldsymbol{u}_h, \boldsymbol{u}_h\rangle = \langle A\boldsymbol{u}_h, \boldsymbol{u}_h\rangle + \langle A_\Gamma\boldsymbol{u}_h, \boldsymbol{u}_h\rangle$$

Noticing $\langle A_\Gamma\boldsymbol{u}_h, \boldsymbol{u}_h\rangle = 4h|\boldsymbol{u}_h|^2_{1,\Gamma_{nb}} \geq 0$, we easily get the first inequality. To prove the other inequality, it is sufficient to prove:

$$\langle A_\Gamma\boldsymbol{u}_h, \boldsymbol{u}_h\rangle \lesssim \langle A\boldsymbol{u}_h, \boldsymbol{u}_h\rangle.$$

By the inverse inequality and the trace theorem of $H^1(\Omega)$, we obtain:

$$\langle A_\Gamma\boldsymbol{u}_h, \boldsymbol{u}_h\rangle = 4h|\boldsymbol{u}_h|^2_{1,\Gamma_{nb}} \lesssim |\boldsymbol{u}_h|^2_{\frac{1}{2},\Gamma_{nb}} \lesssim |\boldsymbol{u}_h|^2_{1,\Omega} \lesssim \langle A\boldsymbol{u}_h, \boldsymbol{u}_h\rangle. \tag{29}$$

Since $\|\cdot\|_{A_L}$ is equivalent to $\|\cdot\|_A$, we conclude the stability of $\langle A_L\boldsymbol{u}, \boldsymbol{v}\rangle$ by that of $\langle A\boldsymbol{u}, \boldsymbol{v}\rangle$. □

Then we study the non-symmetric case A_Q. By the Lax-Milgram Lemma, it sufficies to prove the corcevity and ellipticity of the bilinear form defined by A_Q.

Lemma 3.3. *The bilinear form defined by $\langle A_Q\boldsymbol{u}_h, \boldsymbol{v}_h\rangle$ satisfies the following properties.*

(1) Corcevity:

$$\langle A_Q\boldsymbol{u}_h, \boldsymbol{u}_h\rangle \geq \|\boldsymbol{u}_h\|_A^2, \quad \forall \boldsymbol{u}_h \in \mathbb{V}_h. \tag{30}$$

(2) Ellipticity:

$$\langle A_Q\boldsymbol{u}_h, \boldsymbol{v}_h\rangle \lesssim \|\boldsymbol{u}_h\|_A\|\boldsymbol{v}_h\|_A, \quad \forall \boldsymbol{u}_h, \boldsymbol{v}_h \in \mathbb{V}_h. \tag{31}$$

Proof. The proof of the first part (30) is trivial, since $\vec{A}_Q - \vec{A} = (\vec{D} - \vec{I})\vec{A}$ is semi-positive definite. For the second part:

$$\langle A_Q \boldsymbol{u}_h, \boldsymbol{v}_h \rangle = \langle A\boldsymbol{u}_h, D\boldsymbol{v}_h \rangle \leq \|\boldsymbol{u}_h\|_A \|D\boldsymbol{v}_h\|_A. \tag{32}$$

It suffices to prove $\|D\boldsymbol{u}_h\|_A \lesssim \|\boldsymbol{u}_h\|_A$. To simplify the notation, we replace $\boldsymbol{u}_h$ with $\boldsymbol{u}$. We define $\boldsymbol{u}_{\Gamma_{nb}}$ such that its coordinate vector $\vec{\boldsymbol{u}}_{\Gamma_{nb}} = \vec{I}_{\Gamma_{nb}} \vec{\boldsymbol{u}}$. We can thus write $D\boldsymbol{u} = \boldsymbol{u} + \frac{1}{3}\boldsymbol{u}_{\Gamma_{nb}}$.

We rewrite the A-norm as

$$\|\boldsymbol{u}\|_A^2 = \vec{\boldsymbol{u}}^\intercal \vec{A} \vec{\boldsymbol{u}} = \sum_{i \neq j, \epsilon_{ij} \subset \mathring{\Omega}_h} (u_i - u_j)^2 + \sum_{i \neq j, \epsilon_{ij} \subset \Gamma_{nb}} \frac{3}{4}(u_i - u_j)^2 + \sum_{i \in \Gamma_{nb}} 2u_i^2,$$

where ϵ_{ij} denotes the edge connecting the i, j-th vertices.

We estimate the norm $\|\boldsymbol{u}_{\Gamma_{nb}}\|_A$ as:

$$\|\boldsymbol{u}_{\Gamma_{nb}}\|_A^2 = \vec{\boldsymbol{u}}^\intercal \vec{A} \vec{\boldsymbol{u}} \quad = \sum_{i \in \Gamma_{nb}} u_i^2 + \sum_{i \neq j, \epsilon_{ij} \subset \Gamma_{nb}} \frac{3}{4}(u_i - u_j)^2 + \sum_{i \in \Gamma_{nb}} 2u_i^2 \leq \frac{3}{2}\|\boldsymbol{u}\|_A^2.$$

In the last step, we have use the explicit formula of the stencil (9). By the triangle inequality,

$$\|D\boldsymbol{u}\|_A = \|\boldsymbol{u} + \frac{1}{3}\boldsymbol{u}_{\Gamma_{nb}}\|_A \leq \|\boldsymbol{u}\|_A + \frac{1}{3}\|\boldsymbol{u}_{\Gamma_{nb}}\|_A,$$

we then get $\|D\boldsymbol{u}\|_A \leq (1 + \sqrt{6})/\sqrt{6}\|\boldsymbol{u}\|_A$. □

Since the operator B is the same in all three schemes, by the relation (28) and (30) of the norm defined by A, A_L, and A_Q, the inf-sup condition for B is also satisfied. We summarize as the following theorem:

Theorem 3.4. *Let $\boldsymbol{u}_h, p_h$ be the solution of any MAC scheme (23) , (24) and (20). We have the stability result:*

$$|\boldsymbol{u}_h|_1 + \|p_h\| \lesssim \|\boldsymbol{f}_h\|_{-1,h} \tag{33}$$

In the operator form, $\|\mathcal{L}_h^{-1}\|_{\mathscr{Y}_h \to \mathscr{X}_h} + \|(\mathcal{L}_h^l)^{-1}\|_{\mathscr{Y}_h \to \mathscr{X}_h} + \|(\mathcal{L}_h^q)^{-1}\|_{\mathscr{Y}_h \to \mathscr{X}_h} \leq C$.

3.4. **Consistency of MAC schemes.** In this section, we prove the consistency of MAC schemes using quadratic extrapolation and linear extrapolation. Although the consistency error for boundary stencils is one order lower, using trace theorem, the overall consistency error is second order for the quadratic extrapolation and first order for the linear one in the right norm $\|\cdot\|_{-1,h}$.

3.4.1. *Consistency error of the quadratic extrapolation.* Let us do the truncation error analysis for the near boundary nodes. Again we take the point $(ih, \frac{h}{2})$ for u component as an example. Consider the following Taylor series expansions:

$$u(ih, 0) = u(ih, 0.5h) - u_y(ih, 0.5h)\frac{h}{2} + u_{yy}(ih, 0.5h)\frac{h^2}{8} - u_{yyy}(ih, 0.5h)\frac{h^3}{48} + \mathcal{O}(h^4), \tag{34}$$

$$u(ih, 1.5h) = u(ih, 0.5h) + u_y(ih, 0.5h)h + u_{yy}(ih, 0.5h)\frac{h^2}{2} + u_{yyy}(ih, 0.5h)\frac{h^3}{6} + \mathcal{O}(h^4). \tag{35}$$

Multiplying (34) by 2 and taking summation with (35) yields the following first order approximation

$$-u_{yy}(ih, 0.5h) = -\frac{4}{3}\left(\frac{2u_0 - 3u_1 + u_2}{h^2}\right) + \mathcal{O}(h). \tag{36}$$

Thus the scheme for the momentum equation of u at point 1 in Figure 6 ($y = 0.5h$) is

$$-\frac{4}{3}\cdot\frac{2u_0 - 3u_1 + u_2}{h^2} - \frac{u_3 - 2u_1 + u_4}{h^2} + \frac{p_2 - p_1}{h} = f_1.$$

The scheme derived above for the near boundary points at the top is equivalent to the quadratic extrapolated scheme (24). From the truncation error analysis, it is clear that the quadratic extrapolated MAC scheme (24) is second order at the interior nodes but only first order at the near boundary nodes. However, the difference of $\Pi_h\mathcal{L}\boldsymbol{x}$ and $\mathcal{L}_h^q I_h\boldsymbol{x}$ will still be second order under the weaker norm $\|\cdot\|_{-1,h}$.

For any $\boldsymbol{v}_h \in \mathbb{V}_h$, we denote $\boldsymbol{v}_h := \boldsymbol{v}_{\Gamma_{nb}} + \mathring{\boldsymbol{v}}_h$. It is obvious that $\| \mathring{\boldsymbol{v}}_h \| \leq \|\boldsymbol{v}_h\|$. Following the proof of Lemma 3.3, one can also prove $| \mathring{\boldsymbol{v}}_h |_1 \lesssim |\boldsymbol{v}_h|_1$.

Lemma 3.5. *For a function $\boldsymbol{f} \in \boldsymbol{H}^2(\Omega)$ and its interpolation $\boldsymbol{f}_I$ defined in (19), we have*

$$|(\boldsymbol{f}, \mathring{\boldsymbol{v}}_h) - \langle \boldsymbol{f}_I, \mathring{\boldsymbol{v}}_h\rangle| \lesssim h^2|\boldsymbol{f}|_2\|\boldsymbol{v}_h\|, \quad \text{for any } \boldsymbol{v}_h \in \mathbb{V}_h. \tag{37}$$

Proof. For any interior basis function $\boldsymbol{\phi}_i, i = N_b + 1, N_b + 2, ..., N_u$, we consider the linear functional $\varphi_i(\boldsymbol{f}) = (\boldsymbol{f}, \boldsymbol{\phi}_i) - \langle \boldsymbol{f}_I, \boldsymbol{\phi}_i\rangle = \int \boldsymbol{f}\boldsymbol{\phi}_i - h^2\boldsymbol{f}_i$. Since the support of $\boldsymbol{\phi}_i$ is symmetric, it is easy to check that the functional is bounded, and has zero value on linear functions. By the standard scaling argument and the Bramble-Hilbert lemma, we have $|(\boldsymbol{f}, \boldsymbol{\phi}_i) - \langle \boldsymbol{f}_I, \boldsymbol{\phi}_i\rangle| \lesssim h^2|f|_2$. Then summing up with weight, we have

$$\left|(\boldsymbol{f}, \mathring{\boldsymbol{v}}_h) - \langle \boldsymbol{f}_I, \mathring{\boldsymbol{v}}_h\rangle\right| = \left|\sum_{i=N_b+1}^{N_u}\int \boldsymbol{f}\boldsymbol{v}_i\boldsymbol{\phi}_i - \sum_{i=N_b+1}^{N_u} h^2\boldsymbol{f}_i\boldsymbol{v}_i\right| \lesssim h^2|\boldsymbol{f}|_2\| \mathring{\boldsymbol{v}}_h \|$$

.

□

Lemma 3.6. *Assume $\boldsymbol{u} \in \boldsymbol{H}_0^1(\Omega)\cap W^{3,\infty}(\Omega)$, $\Delta\boldsymbol{u} \in H^2(\Omega)$, and $p \in L_0^2(\Omega)\bigcap W^{3,\infty}(\Omega)$. For $\boldsymbol{x} = (\boldsymbol{u}, p)^\intercal$ and $\Pi_h\boldsymbol{f} = \boldsymbol{f}_I$, we have:*

$$\|\Pi_h\mathcal{L}\boldsymbol{x} - \mathcal{L}_h^q I_h\boldsymbol{x}\|_{\mathscr{Y}_h} \lesssim (\|\boldsymbol{u}\|_{3,\infty} + \|\Delta\boldsymbol{u}\|_2 + \|p\|_{3,\infty})h^2 \tag{38}$$

Proof. For any $\boldsymbol{z}_h = (\boldsymbol{v}_h, q_h) \in \mathscr{X}_h$,

$$|\langle \Pi_h\boldsymbol{y} - \mathcal{L}_h^q\boldsymbol{x}_I, \boldsymbol{z}_h\rangle| = |\langle \boldsymbol{f}_I - \mathcal{L}_h^q\boldsymbol{x}_I, \boldsymbol{v}_h\rangle| + |\langle 0 - \mathcal{L}_h^q\boldsymbol{x}_I, q_h\rangle| := I_1 + I_2.$$

The second term I_2 can be easily estimated as

$$I_2 \leq \|h^{-2}B\boldsymbol{u}_I\|_\infty \sum_{i=N_u+1}^{N_u+N_p} h^2|q_h(x_i)| \lesssim h^2\|\boldsymbol{u}\|_{3,\infty}\|q_h\|.$$

Here we use the fact $h^{-2}B\boldsymbol{u}_I$ is the second order central difference scheme of $-\operatorname{div}\boldsymbol{u}$ at cell centers.

We further split I_1 into $\boldsymbol{u}$ and p parts as

$$I_1 \leq |\langle -(\Delta\boldsymbol{u})_I - A_Q\boldsymbol{u}_I, \boldsymbol{v}_h\rangle| + |\langle (\nabla p)_I - B^\intercal p_I, \boldsymbol{v}_h\rangle| = I_{1u} + I_{1p}.$$

Let $\vec{\boldsymbol{t}}_p$ be the vector representation of $(\nabla p)_I - h^{-2}B^\intercal p_I$. It is easy to verify, by the Taylor series, $\|\vec{\boldsymbol{t}}_p\|_\infty \lesssim h^2\|p\|_{3,\infty}$. Then

$$I_{1p} = (\vec{\boldsymbol{t}}_p, \vec{\boldsymbol{v}}_h)_h \leq \|\vec{\boldsymbol{t}}_p\|_h\|\vec{\boldsymbol{v}}_h\|_h \lesssim h^2\|p\|_{3,\infty}\|\boldsymbol{v}_h\| \lesssim h^2\|p\|_{3,\infty}|\boldsymbol{v}_h|_1.$$

To estimate I_{1u}, we further split it into the sum of near boundary part and interior part.

$$I_{1u} \le |\langle -(\Delta \boldsymbol{u})_I - A_Q \boldsymbol{u}_I, \boldsymbol{v}_{\Gamma_{nb}} \rangle| + |\langle -(\Delta \boldsymbol{u})_I - A_Q \boldsymbol{u}_I, \mathring{\boldsymbol{v}}_h \rangle| = I_{11} + I_{12}.$$

Due to the density of $C^3(\Omega)$ in $W^{3,\infty}(\Omega)$, by the Taylor expansion analysis (36), for the near boundary nodes, i.e., $1 \le i \le N_b$,

$$|(-(\Delta \boldsymbol{u})_I - h^{-2} A_Q \boldsymbol{u}_I)(x_i)| \le Ch \|\boldsymbol{u}\|_{3,\infty}.$$

We can then estimate the near boundary part I_{11} as follows:

$$I_{11} \lesssim h \|\boldsymbol{u}\|_{3,\infty} \sum_{i=1}^{N_b} h^2 |\boldsymbol{v}_h(x_i)| \lesssim h^2 \|\boldsymbol{u}\|_{3,\infty} \|\boldsymbol{v}_h\|_{L^1(\Gamma_{nb})} \lesssim h^2 \|\boldsymbol{u}\|_{3,\infty} |\boldsymbol{v}_h|_1.$$

In the last inequality, we have applied the trace theorem for H^1 functions.

To estimate I_{12}, we interpret the finite difference scheme as the finite element scheme while both methods get the same stencil for the interior part. We have

$$\begin{aligned} I_{12} &= |\langle (\triangle \boldsymbol{u})_I - \triangle \boldsymbol{u}, \mathring{\boldsymbol{v}}_h \rangle + \langle \nabla (\boldsymbol{u} - \boldsymbol{u}_I), \nabla \mathring{\boldsymbol{v}}_h \rangle| \\ &\lesssim h^2 (\|\Delta u\|_2 + \|\boldsymbol{u}\|_3) |\boldsymbol{v}_h|_1. \end{aligned}$$

In the above deducing, we have used Lemma 3.5 and the estimate $|\langle \nabla(\boldsymbol{u} - \boldsymbol{u}_I, \nabla \mathring{\boldsymbol{v}}_h \rangle| \lesssim h^2 \|\boldsymbol{u}\|_3 |\boldsymbol{v}_h|_1$ on uniform grids; see for example [2].

Combining the estimate of I_1 and I_2 we have

$$|\langle \Pi_h \boldsymbol{y} - L_h^q \boldsymbol{x}_I, \boldsymbol{z}_h \rangle| \lesssim h^2 (\|\boldsymbol{u}\|_{3,\infty} + \|\triangle \boldsymbol{u}\|_2 + \|p\|_{3,\infty}) \|\boldsymbol{z}_h\|_{\mathscr{X}_h}$$

and Lemma 38 follows from the definition of the dual norm $\|\cdot\|_{\mathscr{Y}_h}$. □

3.4.2. *Consistency error of the linear extrapolation.* For the near boundary stencil of the linear extrapolated MAC (23), the scheme approximates $-u_{xx} - \frac{3}{4} u_{yy}$ but not $-\Delta u$ at Γ_{nb}^u, which causes the loss of consistency near the boundary.

Lemma 3.7. *Assume $\boldsymbol{u} \in \boldsymbol{H}_0^1 \cap W^{3,\infty}(\Omega), \Delta \boldsymbol{u} \in H^2(\Omega), p \in L_0^2(\Omega) \bigcap W^{3,\infty}(\Omega)$. For $\boldsymbol{x} = (\boldsymbol{u}, p)^\intercal$ and $\Pi_h \boldsymbol{f} = \boldsymbol{f}_I$, we have:*

$$\|\Pi_h \mathcal{L} \boldsymbol{x} - \mathcal{L}_h^l I_h \boldsymbol{x}\|_{\mathscr{Y}_h} \lesssim (\|\boldsymbol{u}\|_{3,\infty} + \|\triangle \boldsymbol{u}\|_2 + \|p\|_{3,\infty}) h \tag{39}$$

Proof. The proof is similar to (38) with the only different term is I_{11} for which

$$|(-(\Delta \boldsymbol{u})_I - h^{-2} A_L \boldsymbol{u}_I)(x_i)| \le C \|\boldsymbol{u}\|_{3,\infty}.$$

Therefore we can get the first order estimate

$$I_{11} \lesssim \|\boldsymbol{u}\|_{3,\infty} \sum_{i=1}^{N_b} h^2 |\boldsymbol{v}_h(x_i)| \lesssim h^2 \|\boldsymbol{u}\|_{3,\infty} \|\boldsymbol{v}_h\|_{L^1(\Gamma_{nb})} \lesssim h \|\boldsymbol{u}\|_{3,\infty} |\boldsymbol{v}_h|_1.$$

□

3.5. **Convergence.** Based on the stability and consistency, we present our main results.

Theorem 3.8. *Let $\boldsymbol{u}_h, p_h$ be the solution of the MAC scheme (24) with quadratic extrapolation, and let $\boldsymbol{u}_I, p_I$ be the nodal interpolation of the solution $\boldsymbol{u}, p$ of Stokes equations. Assume $\boldsymbol{u} \in \boldsymbol{H}_0^1(\Omega) \cap W^{3,\infty}(\Omega), \Delta \boldsymbol{u} \in H^2(\Omega)$, and $p \in L_0^2 \bigcap W^{3,\infty}(\Omega)$. Then*

$$|u_I - u_h|_1 + \|p_I - p_h\| \lesssim (\|\boldsymbol{u}\|_{3,\infty} + \|\triangle \boldsymbol{u}\|_2 + \|p\|_{3,\infty}) h^2$$

Similarly for linear extrapolation MAC, only first order convergence is obtained.

Theorem 3.9. *Let $\boldsymbol{u}_h, p_h$ be the solution of the MAC scheme (23) with linear extrapolation, and let $\boldsymbol{u}_I, p_I$ be the nodal interpolation of the solution $\boldsymbol{u}, p$ of Stokes equations. Assume $\boldsymbol{u} \in \boldsymbol{H}_0^1(\Omega) \cap W^{3,\infty}(\Omega), \Delta \boldsymbol{u} \in H^2(\Omega)$, and $p \in L_0^2 \bigcap W^{3,\infty}(\Omega)$. Then*

$$|u_I - u_h|_1 + \|p_I - p_h\| \lesssim (\|\boldsymbol{u}\|_{3,\infty} + \|\triangle \boldsymbol{u}\|_2 + \|p\|_{3,\infty})h$$

Remark 3.10. Using triangle inequality and interpolation error estimate, we can easily get the first order convergence of linear extrapolation which is equivalent to MAC using co-volume method in Niclaides [5]. In view of approximation theory, first order is already optimal. The second order result for the quadratic extrapolation is known as superconvergence, i.e., two discrete solutions could be more closer.

Using the following discrete embedding theorem (in two dimensions only)

$$\|\boldsymbol{v}_h\|_\infty \lesssim |\log h||v_h|_1,$$

and the second order interpolation error estimate

$$\|\boldsymbol{u} - \boldsymbol{u}_I\|_\infty \lesssim \|\boldsymbol{u}\|_{2,\infty} h^2,$$

we obtain the nearly second order maximum norm for the quadratic extrapolation scheme.

Corollary 3.11. *Let $\boldsymbol{u}_h, p_h$ be the solution of the MAC scheme (24) with quadratic extrapolation. Assume the solution $\boldsymbol{u}, p$ of Stokes equations satisfying $\boldsymbol{u} \in \boldsymbol{H}_0^1(\Omega) \cap W^{3,\infty}(\Omega), \Delta \boldsymbol{u} \in H^2(\Omega)$, and $p \in L_0^2 \bigcap W^{3,\infty}(\Omega)$. Then*

$$\|\boldsymbol{u} - \boldsymbol{u}_h\|_\infty \lesssim (\|\boldsymbol{u}\|_{3,\infty} + \|\triangle \boldsymbol{u}\|_2 + \|p\|_{3,\infty})|\log h| h^2.$$

ACKNOWLEDGMENT

Thanks for Wang Ming for the help on the preparation of the tex file, especially those nice figures.

REFERENCES

[1] A. Brandt and N. Dinar. Multi-grid solutions to elliptic flow problems. Technical Report 79, Institute for Computer Applications in Science and Engineering. NASA Langley Research Center, Hampton, Virginia, New York, 1979.

[2] J. Brandts and M. Krizek. Gradient superconvergence on uniform simplicial partitions of polytopes. *IMA journal of numerical analysis*, 23:489–505, 2003. 15

[3] H. Han and X. Wu. A New Mixed Finite Element Formulation and the MAC Method for the Stokes Equations. *SIAM J. Numer. Anal.*, 35(2):560–571, 1998. 8, 9, 11

[4] F. H. Harlow and J. E. Welch. Numerical calculation of time-dependent viscous incompressible flow of fluid with free surface. *Physics of fluids*, 8(12):2182, 1965. 1

[5] R. A. Nicolaides. Analysis and Convergence of the MAC Scheme. I. The Linear Problem. *SIAM J. Numer. Anal.*, 29(6):1579–1591, 1992. 8, 16